Microemulsions for the Covalent Patterning of Graphene

Alicia Naranjo, Natalia Martín Sabanés, Manuel Vázquez Sulleiro and Emilio M. Pérez*

COMMUNICATION

Microemulsions for the Covalent Patterning of Graphene

Alicia Naranjo,[a] Natalia Martín Sabanés,[a] Manuel Vázquez Sulleiro[a] and Emilio M. Pérez*[a]

Received 00th January 20xx,
Accepted 00th January 20xx

DOI: 10.1039/x0xx00000x

We show that microemulsions can be used as a simple, cheap and scalable template for the covalent patterning of graphene.

Carbon-based nanomaterials have been widely studied due to their unique and useful properties in many different fields.[1-3] Specifically, graphene, as a single layer of sp^2-hybridized carbon atoms bonded in a honeycomb lattice, is known as the thinnest and strongest 2D-material. Graphene is characterized by the lightest charge carriers (massless Dirac fermions) and extraordinary thermal, mechanical and electrical properties.[4-6] These remarkable properties make it useful in a wide range of applications ranging from the mechanical reinforcement of materials[7-9] to building complex sensors.[10-12]

The applicability of graphene could be further enhanced by selective covalent and non-covalent modification, however, tuning the surface or lattice regions to modify its properties is still a challenge, because all the C atoms in graphene (except the edges) are chemically identical. In recent years, many techniques have been developed to pattern 2D-materials, using covalent or non-covalent functionalization.[13] Particularly, nano-patterning has evolved as a possibility to overcome the chemoselectivity problem. One of these approaches relies on electron beam lithography followed by covalent patterning to carry out a precise positioning of organic functional groups on the basal plane of graphene at a micro scale.[14] The main drawback of this approach is the need to use a combination of top-down and bottom-up strategies, which implies long production times and the presence of residual e-beam resist. Another approach relies on exploiting the Moiré patterning that emerges from the growth of graphene on metallic substrates as a template for the subsequent formation of C-C bonds.[15, 16] More recent techniques for nano-patterning have been developed using laser writing. This approach reckon on laser-triggered photolysis for the selective and reversible patterning of graphene, involving silver nanoparticles to generate trifluoromethyl radicals, requiring of an external source for a laser-induced patterning.[17-20] While these approaches represents the ultimate degree in control with regards to resolution down to atomic scale, they all require complicated nanofabrication techniques and equipment. Recently, self-assembled molecular networks have been used to achieve patterning with few nm periodicity, partly overcoming this problem, but relying instead on a very specific molecular design.[21]

The design of a biphasic system with controlled size of the phases, an emulsion (EM), could be used as an alternative method for functionalization patterns in 2D-materials. Microemulsions (MEMs) are a mixture of two immiscible liquids in which one is dispersed in spherical droplets of 100-1000 nm into the other.[22-24] The presence of amphiphilic molecules allows the formation of micelles in the liquid phase and controls the dispersibility. The hydrophilic-lipophilic balance (HLB) of the surfactant is a measure of the affinity towards oil or water and it determines the miscibility of the different liquids.[25] Consequently, MEMs structures can be defined by low HLB values in which droplets of water are dispersed in oily media (W/O) or high HLB values which are held by oily micelles into aqueous media (O/W).[26] MEMs are considered as kinetically stable dispersions,[27] and dynamic light scattering (DLS) is often used to fully characterize the droplet size and polydispersity index.[28] MEMs can be prepared by two methodologies:[29] i) high-energy methods[24, 26] using ultrasonic emulsification,[30, 31] high pressure homogeniser[32, 33] or high shear mixer; and ii) low-energy methods using phase inversion temperature,[34-36] self-assembling nano-emulsification or spontaneous nano-emulsification.[37]

Introducing organic molecules inside of a biphasic system during the formulation process could arrange a selective patterning of surfaces. Different systems can be designed where the organic compounds lie inside or outside the MEMs droplets, depending on solubility. Potentially, simultaneous bifunctionalization could be achieved by designing MEMs with different molecules in and outside of the droplets.

Here, we report a method for covalent patterning of graphene on SiO_2 substrates, using MEMs as a template. The method is carried out at room temperature, using cheap, commercially available solvents and surfactants, and would therefore be easily scalable.

Blank MEMs (without organic compound) were synthesized by dispersing an aqueous phase (AP), into an oily phase (OP) by using a pump with a rate of 1mL/min under vigorous stirring for 30 minutes

[a] IMDEA Nanociencia, C/Faraday 9, Ciudad Universitaria de Cantoblanco, 28049 Madrid, Spain.

† Electronic Supplementary Information (ESI) available: Experimental data, Figure S1-11. See DOI: 10.1039/x0xx00000x

at 80 °C (resulting in an emulsion, EM in Figure 1). This was followed by 45 minutes of sonication at r.t. to homogenize the samples and achieve the microscale droplet size (MEM in Figure 1).

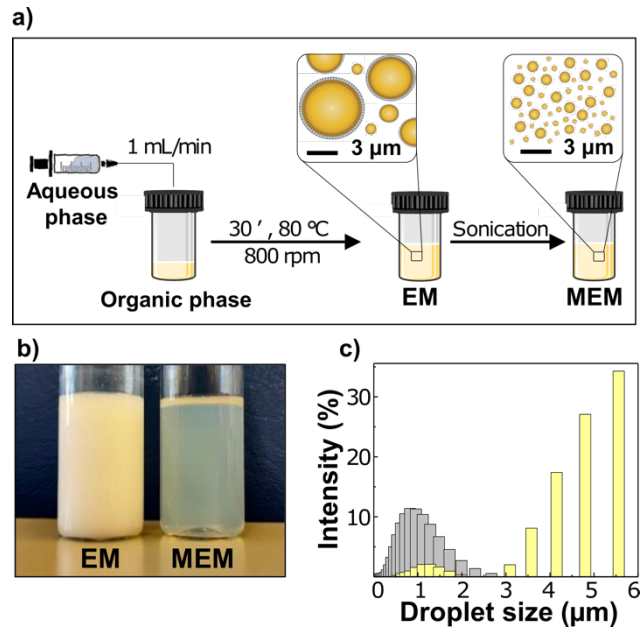

Figure 1. a) Scheme of the microemulsion (MEM) formulation; b) optical image comparing EM versus MEM; c) droplet size distribution of EM (yellow bars) and MEM (grey bars) obtained by DLS.

Optical images and particle size of the resulting (M)EMs through the different synthetic steps can be found in Figure 1b and 1c, respectively. Further experimental details on sample preparation and characterization can be found in Supporting material, SI, section 1.

To prepare patterning MEMs (containing organic compound inside), 2 mg of 4-Bromobenzenediazonium tetrafluoroborate were added to the blank MEMs after the sonication step in MEM preparation. This mixture was sonicated for some minutes until salt was dissolved. Separate experiments with the oil and aqueous phases, showed that the diazonium salt is very soluble in the aqueous phase (ca. 80 mg/mL in water + T80) while it is much less soluble in the oil phase (ca. 7 mg/mL), as expected (SI section 2, Figure S1). Droplet size and polydispersity index (PDI) of all prepared MEMs (blank and patterning) were assessed at room temperature without dilution, via DLS measurements (SI, section 1). The blank MEMs are formed by micelles of 710 ± 78 nm with a PDI of 0.29 ± 0.04, Figure 2. A proper homogeneity was observed, both in DLS data and microscopy images. Besides, no differences were found in the case of the presence of the diazonium salt inside of the emulsion (Figure 2a).

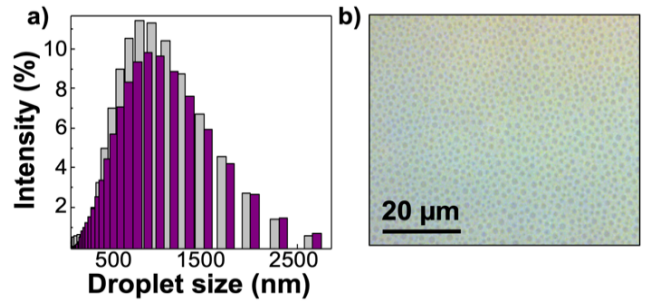

Figure 2. a) Distribution of the droplet size from two kind of MEMs: blank MEM (without organic compound) in grey, diazonium salt MEM (with organic compound) in purple. b) Microscopy images of the sample (drop-casted onto a glass slide), representing droplets of 700nm.

Cryo-SEM studies were also performed (SI, section 1). The average droplet size extracted from the SEM micrographs fit the data obtained by DLS, (SI section 3, Figure S2).

The content of the MEMs droplets was studied by Raman spectroscopy by drop-casting the MEMs onto a glass slide. Oil and T80 commercial solutions are previously studied to assign the corresponding bands, allowed us identifying the material inside of the droplets, (see details in SI section 4, Figure S3). Raman results confirm that oily micelles are dispersed in an aqueous media, due to the absence or presence of a band at 1654 cm^{-1}, characteristic of the T80 surfactant dissolved in the aqueous phase (SI section 4, Figures S4 and S5). The size of the oily micelles in the Raman maps is 14 ± 2 µm in diameter, in good agreement with the sizes obtained for the droplets in liquid (around 710 ± 78 nm). Due to the deposition into a flat surface (glass slide), we expect the droplets to lose the spherical shape and collapse into disk-shaped bubbles that in this case would present around 1.2 nm height.

The same characterization process was used for blank and patterning samples, showing no notable difference between samples in terms of size and distribution of droplets in the MEMs or Raman characterization. The Raman spectra do not show any fingerprint of the diazonium salt itself, likely covered by the strong signals of the T80 surfactant (more detailed information in SI, section 4).

The MEMs with diazonium salt were used to test the selective functionalization of graphene substrates. To that end, graphene substrates were submerged in the MEMs solution for 5 minutes, then washed several times in water and finally dried with a nitrogen flow (Figure 3). Three different samples were studied according to the functionalization grade: a) pristine graphene substrates, (pr-G), with no functionalization; b) fully functionalized graphene substrates, (f-G), using a 4mM aqueous solution of the diazonium salt for the functionalization process and c) patterned graphene substrates, (p-G), which implies functionalization by MEM-patterning (see SI section 1 for details on sample preparation). Raman spectroscopy was used to characterize the functionalization using a 532 nm laser excitation. The relative intensity of the defect-induced D band (at 1348 cm^{-1}) with respect to the G band (at 1598 cm^{-1}) directly indicates the degree of functionalization.[38, 39] Higher functionalization results in an increase in the I_D/I_G ratio, and vice versa, unfunctionalized graphene show low presence of defects and low I_D/I_G ratio.

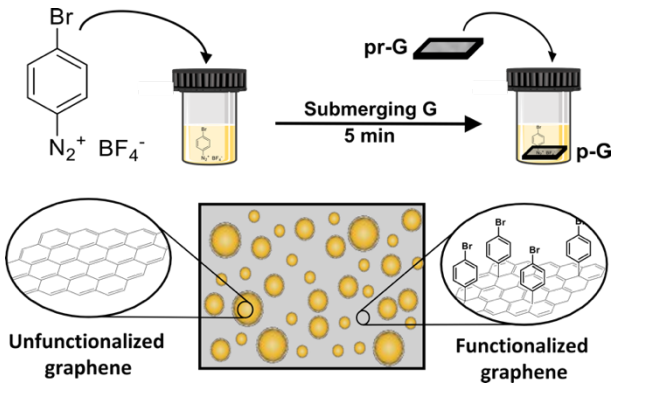

Figure 3. Scheme of the patterning process by submerging graphene substrate in patterning MEMs.

Figures 4a, b and c show Raman maps of the I_D/I_G ratios for pr-G, f-G and p-G samples, respectively. Characteristic Raman spectra for each sample are shown in Figure 4d (details in Figure S6, section 5). First, we see that the functionalization reaction works well under our conditions, as reflected in an increase in the I_D/I_G ratio from 0.05 ± 0.03 (pr-G) to 1.85 ± 0.24 in the fully functionalized control experiments (f-G). Moreover, we see that the functionalization in this case is relatively homogeneous with very small variations in the maps in those cases (lighter purple and orange spots in the pr-G and f-G samples, respectively). These are assigned to defects in the purchased graphene substrates (SI section 6, Figure S7 and S8).

In the case of p-G substrates (Figure 4c), both functionalized and unfunctionalized graphene areas are found. Spherical non-patterned areas (dark purple zones with low I_D/I_G ratio) are observed with sizes in the 10 μm range, matching the oily droplets measured by Raman in a glass substrate (SI, Figures S4 and S5 and discussion above). The functionalized areas (orange zones with an increased D band), correspond to the aqueous regions containing the diazonium salt in the MEMs. Quantitatively, statistical analysis of the Raman spectra in the dark purple versus dark orange areas show an increase of the D band on patterned areas with I_D/I_G = 0.82 ± 0.01, against non-patterned zones where I_D/I_G = 0.37 ± 0.08 in average (details in SI section 7, Figure S9).

Statistical distributions of the I_D/I_G ratio for pr-G, f-G and p-G samples can be found in SI (Figure S10, section 7). Both fully functionalized and patterned samples show a wider distribution of intensity ratios in comparison with the pristine sample. In the case of the patterned substrate, (p-G), this is a clear consequence of the different degrees of functionalization over the sample, while for the f-G sample it reflects the presence of non-functionalized defects in the pristine substrate. In addition to the I_D/I_G ratio changes, Raman shifts of the G and 2D modes are also observed on the patterned samples (Figure 5). The areas showing a higher I_D/I_G ratio (orange in Figure 4d) also show significant blue shifts of the G (from ca. 1591 cm^{-1} to 1597 cm^{-1}) and 2D modes (from ca. 2682 cm^{-1} to 2691 cm^{-1}).

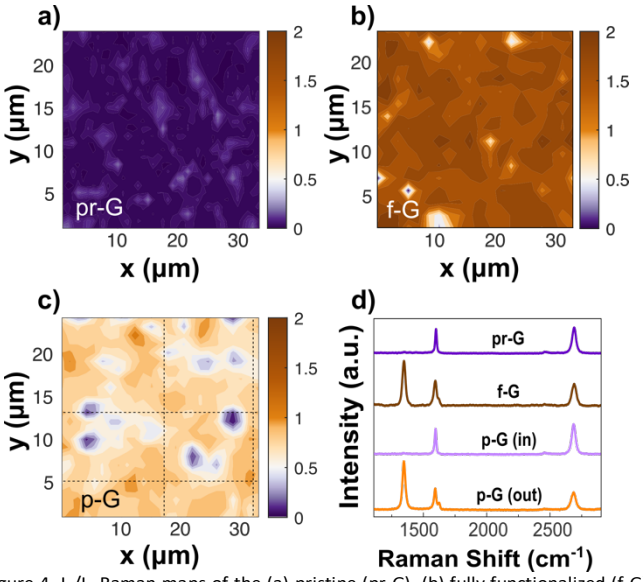

Figure 4. I_D/I_G Raman maps of the (a) pristine (pr-G), (b) fully functionalized (f-G) and (c) patterned (p-G) graphene substrates. d) Raman spectra of the different samples (pr-G, f-G and p-G), including two different zones on p-G due to the patterning process (inside and outside the purple droplets).

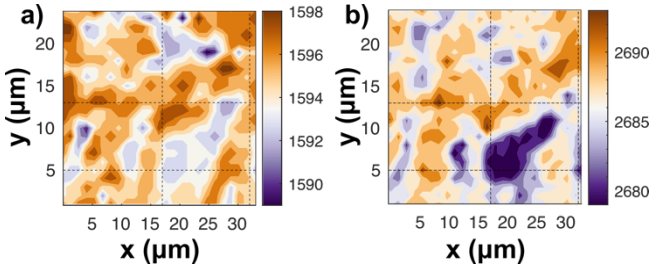

Figure 5. Maps of the Raman shift of the G (a) and 2D (b) modes of graphene for the patterned (p-G) sample in the same area depicted in Figure 4. Dashed lines are guides to the eye to localize different areas and facilitate comparison with figure 4d.

Since the graphene substrate is supported on SiO_2, and all measurements are carried out at room temperature, significant changes on the mechanical strain on the graphene substrate can be ruled out, and these shifts can be safely ascribed to doping of the graphene sample.[40, 41] In other words, the covalent patterning results in a spatial modulation of the electronic properties of graphene, as intended.

In summary, we report a simple yet effective method to pattern graphene covalently by using microemulsions, with micrometric resolution. We also show that the covalent patterning results in a periodic variation in the electronic structure of the 2D-material that corresponds spatially with the chemical functionalization, which is arguably the ultimate goal of this kind of chemical methods. The biphasic nature of MEMs constitutes a perfect platform for patterning 2D-materials, where the droplet size and content can be tuned to customize the grafting. As a proof-of-principle example of this tunability, we performed experiments with a MEM of significantly smaller droplet size, under otherwise identical conditions, and successfully obtained patterning at a smaller scale (see the SI, Figure S11). Exploring variations in droplet sizes, the molecular content within each phases, the differences in wettability, and the various reactions (covalent and noncovalent) developed for 2D materials on substrates,[38, 42] can result in an easy and scalable methodology to extend this concept to applications where large-area patterning is required, and is currently our next objective.

Acknowledgements

E.M.P. acknowledges the MINECO (CTQ2017-86060-P; PID2020-116661RB-I00), and Comunidad de Madrid (P2018/NMT-4367). IMDEA Nanociencia receives support from the "Severo Ochoa" Programme for Centres of Excellence in R&D (MINECO, Grant SEV-2016-0686). N.M.S. acknowledges the MSCA program MSCA-IF-2019-892667.

Notes and references

1. P. Avouris, Z. Chen and V. Perebeinos, *Nat. Nanotechnol.*, 2007, **2**, 605-615.
2. V. Georgakilas, J. N. Tiwari, K. C. Kemp, J. A. Perman, A. B. Bourlinos, K. S. Kim and R. Zboril, *Chem. Rev. (Washington, DC, U. S.)*, 2016, **116**, 5464-5519.

3. D. Jariwala, V. K. Sangwan, L. J. Lauhon, T. J. Marks and M. C. Hersam, *Chem. Soc. Rev.*, 2013, **42**, 2824-2860.
4. A. K. G. a. K. S. Novoselov, *Nature Materials*, 2009, **6**, 11-19.
5. V. C. T. a. R. B. K. Matthew J. Allen, *Chem. Rev.*, 2010, **110**, 132-145.
6. K. S. Novoselov, V. I. Fal'ko, L. Colombo, P. R. Gellert, M. G. Schwab and K. Kim, *Nature (London, U. K.)*, 2012, **490**, 192-200.
7. X. Huang, X. Qi, F. Boey and H. Zhang, *Chem. Soc. Rev.*, 2012, **41**, 666-686.
8. P. Wang, Q. Cao, Y. Yan, Y. Nie, S. Liu and Q. Peng, *Nanomaterials*, 2019, **9**, 59/51.
9. V. D. Ho, C.-T. Ng, C. J. Coghlan, A. Goodwin, C. Mc Guckin, T. Ozbakkaloglu and D. Losic, *Constr. Build. Mater.*, 2020, **234**, 117403.
10. A. Martin-Pacheco, A. E. Del Rio Castillo, C. Martin, M. A. Herrero, S. Merino, J. L. Garcia Fierro, E. Diez-Barra and E. Vazquez, *ACS Appl Mater Interfaces*, 2018, **10**, 18192-18201.
11. H. Pei, J. Li, M. Lv, J. Wang, J. Gao, J. Lu, Y. Li, Q. Huang, J. Hu and C. Fan, *Journal of the American Chemical Society*, 2012, **134**, 13843-13849.
12. Q. Wu, Y. Qiao, R. Guo, S. Naveed, T. Hirtz, X. Li, Y. Fu, Y. Wei, G. Deng, Y. Yang, X. Wu and T.-L. Ren, *ACS Nano*, 2020, **14**, 10104-10114.
13. Y. Zhou and K. P. Loh, *Advanced Materials*, 2010, **22**, 3615-3620.
14. M. C. Rodriguez Gonzalez, A. Leonhardt, H. Stadler, S. Eyley, W. Thielemans, S. De Gendt, K. S. Mali and S. De Feyter, *ACS Nano*, 2021, **15**, 10618-10627.
15. J. J. Navarro, S. Leret, F. Calleja, D. Stradi, A. Black, R. Bernardo-Gavito, M. Garnica, D. Granados, A. L. Vazquez de Parga, E. M. Perez and R. Miranda, *Nano Lett.*, 2016, **16**, 355-361.
16. J. J. Navarro, F. Calleja, R. Miranda, E. M. Pérez and A. L. V. d. Parga, *Chem. Commun.*, 2017, **53**, 10418--10421.
17. K. F. Edelthalhammer, D. Dasler, L. Jurkiewicz, T. Nagel, S. Al-Fogra, F. Hauke and A. Hirsch, *Angew. Chem., Int. Ed.*, 2020, **59**, 23329-23334.
18. T. Wei, S. Al-Fogra, F. Hauke and A. Hirsch, *J. Am. Chem. Soc.*, 2020, **142**, 21926-21931.
19. L. Bao, B. Zhao, M. Assebban, M. Halik, F. Hauke and A. Hirsch, *Chem. - Eur. J.*, 2021, **27**, 8709-8713.
20. T. Wei, X. Liu, S. Al-Fogra, J. Bachmann, F. Hauke and A. Hirsch, *Chem. Commun. (Cambridge, U. K.)*, 2021, **57**, 4654-4657.
21. K. Tahara, Y. Kubo, S. Hashimoto, T. Ishikawa, H. Kaneko, A. Brown, B. E. Hirsch, S. D. Feyter and Y. Tobe, *Journal of the American Chemical Society*, 2020, **142**, 7699-7708.
22. D. J. McClements, *Soft Matter*, 2012, **8**, 1719-1729.
23. B. R. Choradiya and S. B. Patil, *Journal of Molecular Liquids*, 2021, **339**, 116751.
24. E. V. Y. M. Yu Koroleva, *Russian Chemical Reviews*, 2012, **81**, 21-43.
25. S. N. Kale and S. L. Deore, *Systematic Reviews in Pharmacy*, 2016, **8**, 39-47.
26. P. Balamohan, C. H. Anjali and A. Ravindran, *Journal of Bionanoscience*, 2013, **7**, 323-333.
27. P. Fernandez, V. André, J. Rieger and A. Kühnle, *Colloids and Surfaces A: Physicochemical and Engineering Aspects*, 2004, **251**, 53-58.
28. V. Klang, N. B. Matsko, C. Valenta and F. Hofer, *Micron*, 2012, **43**, 85-103.
29. S. Kentish, T. J. Wooster, M. Ashokkumar, S. Balachandran, R. Mawson and L. Simons, *Innovative Food Science & Emerging Technologies*, 2008, **9**, 170-175.
30. V. Ghosh, A. Mukherjee and N. Chandrasekaran, *Ultrason Sonochem*, 2013, **20**, 338-344.
31. T. S. Leong, T. J. Wooster, S. E. Kentish and M. Ashokkumar, *Ultrason Sonochem*, 2009, **16**, 721-727.
32. C. Qian and D. J. McClements, *Food Hydrocolloids*, 2011, **25**, 1000-1008.
33. H. S. a. H. S. Michael Stang, *Engineering in Life Sciences*, 2001, **4**, 151-157.
34. Y. Nonomura and N. Kobayashi, *J Colloid Interface Sci*, 2009, **330**, 463-466.
35. I. Sole, C. M. Pey, A. Maestro, C. Gonzalez, M. Porras, C. Solans and J. M. Gutierrez, *J Colloid Interface Sci*, 2010, **344**, 417-423.
36. D. Song, W. Zhang, R. K. Gupta and E. G. Melby, *AIChE Journal*, 2011, **57**, 96-106.
37. K. Bouchemal, S. Briancon, E. Perrier and H. Fessi, *Int J Pharm*, 2004, **280**, 241-251.
38. A. Criado, M. Melchionna, S. Marchesan and M. Prato, *Angew. Chem., Int. Ed.*, 2015, **54**, 10734-10750.
39. L. M. Malard, M. A. Pimenta, G. Dresselhaus and M. S. Dresselhaus, *Phys. Rep.*, 2009, **473**, 51-87.
40. J. E. Lee, G. Ahn, J. Shim, Y. S. Lee and S. Ryu, *Nat Commun*, 2012, **3**, 1024.
41. M. Kalbac, A. Reina-Cecco, H. Farhat, J. Kong, L. Kavan and M. S. Dresselhaus, *ACS Nano*, 2010, **4**, 6055-6063.
42. S. Bertolazzi, M. Gobbi, Y. Zhao, P. Samori and C. Backes, *Chem Soc Rev*, 2018, **47**, 6845-6888.